CHAPTER 3

Fabrication of SPR biosensor and a measurement prototype to study biomolecular interaction

Contents

Chapter 3: Fabrication of SPR biosensor and a measurement prototype to study biomolecular interaction

3.1 Introduction

This chapter provides a review of the various biosensing platforms and measurement prototypes for the study of biomolecular interactions. Thereafter the chapter presents the fabrication of SPR biosensors and a custom-made SPR measurement prototype for the investigation of biomolecular interactions. Simultaneous detection of various biomolecular interactions using SPR requires the use of microfluidic platforms for the patterning of multiple targets such as proteins, nucleic acids etc. Polymer based microfluidic systems involving Polydimethylsiloxane (PDMS) are increasingly used for several biochemical and biomedical related applications. The bonding of the PDMS microfluidic flow cell with the plasmonic metal (Au) film is a critical step in the fabrication of the SPR biosensors because, unlike the bonding of PDMS with glass, the attachment of PDMS with gold (Au) surface is challenging [1, 2]. A novel bonding technique is used in this research work to ensure irreversible and leakage-free bonding of PDMS microchannels with Au coated glass substrates at room temperature for the construction of SPR biosensors. Following the successful proof of concept with standard proteins, the research further continued with the fabrication of SPR biosensors for the detection of crude snake venom protein. The performance of the biosensors was determined in terms of the sensitivity, selectivity, Limit of Detection (LoD) etc.

Over the past few decades, several methodologies and techniques have been reported in the literature for the study of biomolecular interactions. Enzyme based immunoassays such as Enzyme-linked Immunosorbent Assay (ELISA) are the most widely approaches in this regard producing high sensitivity and LoD. However, the enzyme based approaches not only have drawbacks with regard to cross-reactivity, but also require sophisticated instruments, complex and skilled laboratory procedures characterized by quite a long time to result, labelling tags etc. [3]. Radioimmunoassay (RIA) is a very reliable and sensitive assay requiring fewer processing steps and smaller volumes of samples, however, it is very expensive and hazardous due to the involvement of handling of radioisotopes [4]. Lateral Flow Assay (LFA)/Immunochromatographic techniques despite being sensitive generally require a large volume of reagents, labels and a number of sample pretreatment steps requiring trained professionals and hence do not suit the purpose of point-of-care diagnosis, particularly in rural regions [5]. Colorimetric assays, although simple, fast and economical are not highly sensitive and are easily affected by pH of a solution [6]. The electrochemical methods reported for the

detection of protein, despite their high sensitivities, are subjected to electromagnetic interference and require labelled antibodies, enormous amounts of chemicals in electrochemical cells etc. [7]. Other techniques such as Polymerase Chain Reaction (PCR), although reliable and sensitive, are very time-consuming involving expensive sequencing costs and multiple handling steps prone to contamination [8, 9]. Optical techniques like Immunofluorescence assays and Surface-Enhanced Raman Spectroscopy (SERS) are usually highly sensitive but the use of labelling tags leading to false signalling, requirement of expensive Raman spectrometer, background noise and repeatability issues makes them unfavourable [10, 11]. Localized Surface Plasmon Resonance (LSPR) based methods produce a high Full Width at Half Maximum (FWHM) due to the varying sizes of the nanoparticles leading to inaccurate monitoring of the resonance condition. In this regard, SPR serves as a rapid, facile, reliable and cost-effective approach with high sensitivity and selectivity for the study of biomolecular interaction. The Refractive Index (RI)-sensing transduction mechanism of SPR provides rapid, sensitive and real-time information, without the need for washing and labelling steps, requiring minute amounts of analytes advantageous for clinical applications.

SPR allows the simultaneous study of various biomolecular interactions, particularly important for the analysis of complex biomolecules such as proteins. This requires the use of microfluidic technology for the patterning of multiple proteins so that the target analyte flows through the sensor surface and simultaneously reacts with multiple ligands immobilized on it. Microfluidic platforms are used as biochemical analytical tools for the patterning of protein microarrays, manipulation and analysis of biological cells, separation and detection etc. finding applications in a variety of fields such as drug discovery, food safety etc. and offering the benefits of requirement of lesser volumes of ligands and analytes, precise fluidic control etc. [1, 12-14]. PDMS is a popular choice of material used for the design and fabrication of microfluidic devices owing to its biocompatibility, non-toxicity, optical transparency, chemical inertness etc. [15, 16]. The bonding of the PDMS microfluidic flow cell with plasmonic metal (Au) film is a critical step in the construction of SPR biosensors. This is because unlike the intrinsic properties of PDMS allows its adhesion to silicon-based surfaces such as silicon or glass very easily using plasma treatment, the application of plasma results in the observable damage of the plasmonic film (Au) strongly limiting its utility for bonding PDMS with Au. Thus, the attachment of PDMS with Au poses a challenge [2].

Few SPR microfluidic based biosensing platforms and biosensors have been fabricated over the years for the study of biomolecular interactions. Among such works, most authors reported the detection of biomolecular interaction on microfluidic platforms, involving primarily a single set of analyte-ligand pairs. Zhang *et.al* and Li *et.al.* reported the interaction of Mouse Immunoglobulin-G (IgG) with Goat anti Mouse IgG [17, 18]. Few authors have reported the detection of IgG, pathogens etc. using SPR platforms consisting of rotational stages [19, 20]. Although the use of rotational stages such as goniometers ensures high angular resolutions, they usually are accompanied by an increase in system complexity, large device size and cost. The requirement of expensive goniometric stages and photodetector arrays was eliminated using double-prism configured SPR prototypes as reported by some authors [21, 22]. Although the second prism aids in keeping the plasmon excitation spot and the reflected beam stationary, the achievable angular resolutions were not sufficiently high and also it uses complex optics.

In comparison to the investigation of protein-protein interactions involving standard proteins such as IgG, the pathophysiology of snake venom proteins is very complex due to the diverse protein families present in the venom. These diverse proteins contribute to the neurotoxic effects and haemostatic disruptions observed in snake bite patients after snake envenomation. Snake envenomation is a neglected public health concern leading to deaths and long-term impairments around the world, mostly in tropical and subtropical nations. India is a prime location for snake envenomation with the highest cases reported (81,000) per year, particularly in the rural regions, resulting in approximately 35,000-50,000 casualties [23]. Several species such as Spectacled cobra (*Naja naja*), Saw-scaled viper (*Echis carinatus*), Common krait (*Bungarus caeruleus*), Russell's viper (*Daboia russelii*), and, Monocled cobra (*Naja kaouthia*), Banded krait (*Bungarus fasciatus*), Hump-nosed pit viper (*Hypnale hypnale*), Green pit viper (*Trimeresurus sp.*) etc. are among the more than 52 species of venomous snakes found in the Indian subcontinent [24]. However, *Naja naja*, *Daboia russelii*, *Echis carinatus* and *Bungarus caeruleus*, commonly known as the 'Big Four' are largely responsible for the majority of snakebite incidents in this region [25, 26]. Failure of urgent treatment of snakebite can prove to be fatal due to multiple organ failure. The efficacy of snakebite therapy relies on the distinctive identification of the responsible snake species and the prompt administration of monovalent antivenom specific to the venom. However, visual

identification of the responsible snake is a challenging task and consequently, polyvalent antivenom, which neutralizes venoms from more than one species of snake prevalent in the area of usage, is preferred over monovalent antivenom [27]. In India, the commercially available polyvalent antivenom is raised against the 'Big Four' snakes. However, polyvalent antivenoms have various drawbacks like anaphylactic shock, adverse reactions and inefficiency [28]. Therefore, rapid and reliable approaches are sought after for the detection of snake venom protein, which eliminates the need for sophisticated and expensive instrumentation, complex sample processing steps and large volumes of reagents, particularly for use in impoverished areas where inhabitants typically experience a higher frequency of snakebites.

3.2 Materials and Methodology

The SPR biosensors, in this research work, were fabricated using a novel bonding protocol to ensure the leakage-free bonding of PDMS microchannels with Au substrates for the construction of a multiple protein-patterned biosensor and study its interaction capacity with a target antigen. Figure 3.1 presents a schematic representation of the structure of the SPR biosensor and the process flow of the fabrication. The structure of the sensor primarily consists of a PDMS based microfluidic flow cell and Au coated glass substrate bonded together and immobilized with antibody proteins to form a multiple protein-patterned SPR biosensor. For the fabrication of the biosensors, first, PDMS multichannel microfluidic flow cells were fabricated using a standard technique from a master mould followed by surface functionalization. Second, thin films of Au were deposited on glass substrates followed by surface functionalization and activation. Then the functionalized PDMS were bonded with the activated Au substrates. Thereafter, polyclonal antibodies viz; Mouse anti Human Immunoglobulin-G (M-aHIgG), Goat anti Human Immunoglobulin-G (G-aHIgG) and Rabbit anti Human Immunoglobulin-G (R-aHIgG) of different concentrations, prepared in PBS were injected through the inlets of the PDMS microchannels and immobilized over the surface activated Au substrates for the fabrication of the multiple protein-patterned SPR biosensors. The immobilized antibodies were exposed to different concentrations of target antigen Human Immunoglobulin-G (H-IgG). A custom-made SPR measurement prototype was designed and fabricated to investigate the interaction capacity of the SPR biosensors. Thereafter, following the successful proof of concept with standard proteins, the research further continued with the fabrication of SPR biosensors to detect complex crude snake venom

proteins of *Naja naja* and *Daboia russelii.* The SPR biosensors were constructed by immobilizing polyvalent antivenom and exposed to different concentrations of crude snake venoms.

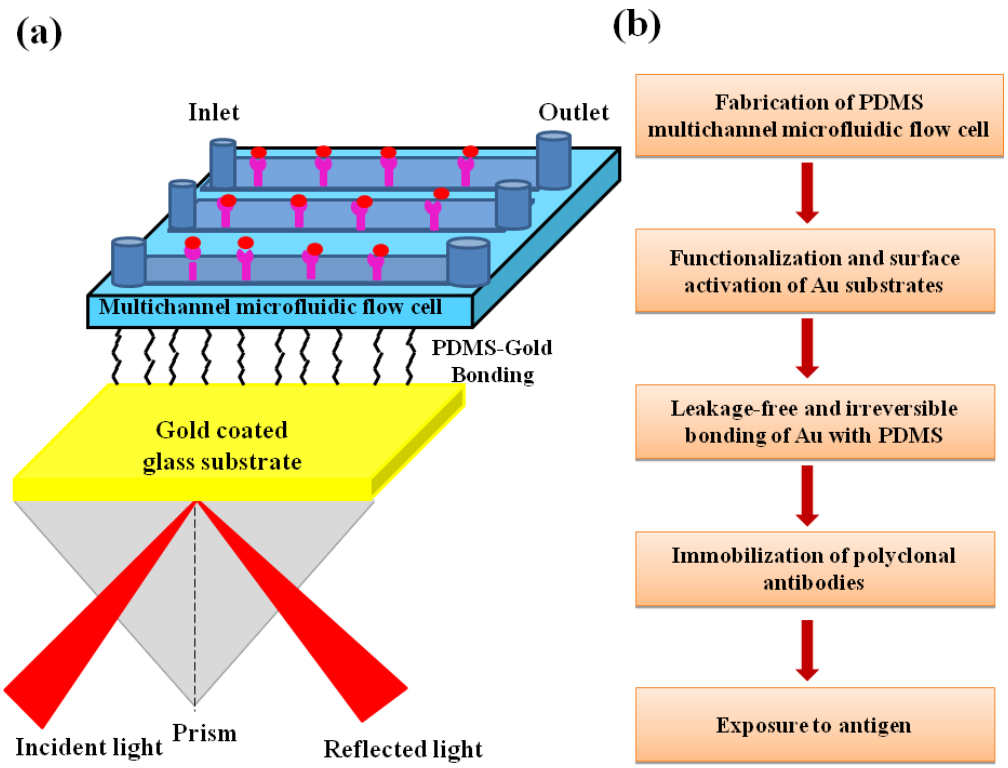

Figure 3.1: Schematic representation of (a) Structure of the SPR biosensor and (b) Process flow of the biosensor fabrication

3.2.1 Materials and Reagents

BK-7 prism (RI 1.515), Laser source (633 nm), Polarizer and RI matching liquid were procured from Edmund Optics, Singapore. One dimensional Complementary Metal Oxide Semiconductor (CMOS) linear image sensor (S9227-04, 512 pixel) was purchased from Hamamatsu Phonics, Japan.

Sylgard 184, 11-Mercuptoundecanoic acid (MUA), 1-ethyl-3 (3-dimethylaminopropyl) carbodiimide (EDC), N-hydroxysuccinimide (NHS), Ethanolamine, Phosphate-Buffered Saline (PBS) were obtained from MilliporeSigma, USA. M-aHIgG, G-aHIgG, R-aHIgG and H-IgG were purchased from GeNei, Bangalore, India. 3-Aminopropyltrimethoxysilane (APTMS) was procured from Thermo Fisher Scientific, USA. Lyophilised crude venom of Indian cobra (*Naja naja*) and Russell's viper (*Daboia russelii*) were purchased from Irula Snake Catchers Industrial Co-operative Society, Mamallapuram, Tamil Nadu, India. Lyophilised Polyvalent

Antivenom was obtained from VinsBioproducts Limited, Telangana, India. Ultra pure Deionised (DI) water was used throughout the experiments. The raw chemicals were of analytical grade and used without further purification.

3.2.2 SPR measurement prototype

The schematic representation of the portable Kretschmann angular configured SPR measurement prototype is shown in Figure 3.2. A miniaturized and robust construction was focused to eliminate any possible handling errors, errors due to vibration etc. Special interest was given to ensure high precision, wide angular scanning range and synchronous movement of light source and detector to eliminate the conventional requirement of expensive goniometric stages and detector arrays. The modeling of the device was done in Pro Engineer software based on which the appropriate design of optical mounts, Allen bolts etc, were chosen and fabricated. The overall mechanical structure and the mounts for optical components were fabricated in a Computer Numerical Control (CNC) lathe machine (MTAB, Model: MAXTURN) and the material used was nylon. A horizontal beam (250 mm length) was hinged to two vertical supports (250 mm length) on either side, standing atop a base of nylon sheet. A removable mould (Figure 3.2a) fabricated for positioning a triangular prism (BK-7, 30 mm x 30 mm x 42.4 mm) was hinged to the horizontal beam. Removable moulds (Figure 3.2b) were also fabricated for mounting a laser (633 nm, 5 mW, 36 mm length) and a CMOS linear image sensor (512 pixel). An Allen Bolt (12 mm diameter, 120 mm length) was coupled to the shaft of a microcontroller controlled stepper-motor (3.2 Kg-cm torque) positioned beneath the nylon sheet. Two hemispherical stages (Figure 3.2c) constructed for supporting the mould of the laser/image sensor were connected to an 'H-shaped' block (Figure 3.2d) embedded in the Allen Bolt. The stages connected to the two arms guided the angular movement of the laser/image sensor and ensured that the laser spot on the sensor chip was stationary throughout the angular movement. The stationary position of the prism also ensured that the incident angle was equal to the reflected one for a wide angular scanning range of 30˚-80˚. The prototype measures 300 mm x 250 mm x 250 mm in dimension weighing ~3.5 kg.

While conducting measurement, the prism with its apex facing downwards was mounted on the mould and the laser and the image sensor were mounted over the two hemispherical stages facing each other. In order to minimize the optical transmission

loss, a few drops of index matching liquid (RI=1.51, Norland Optical Adhesive) were poured on the flat surface of the BK 7 prism (RI=1.515) and the SPR biosensor was placed over it with the BK 7 glass substrate facing downwards. The shaft of the programmable stepper-motor was used to turn Allen Bolt in the clockwise direction causing the 'H-shaped' block to move upwards, which in turn resulted in synchronized angular increment of the laser and the image sensor. The SPR biosensor was illuminated by a laser source (633 nm) passing through the glass prism under the conditions of total internal reflection and the reflected light from the biosensor was captured using a detector (CMOS linear image sensor, 512 pixel). The clock and timing signals to the linear CMOS image sensor were provided using a microcontroller which receives the signal voltages from the detector, performs analog-to-digital conversion and serially transmits it to the computer. The collected data were used for the analysis of resonance condition. All the calibration measurements as well as the validation experiments were carried out at room temperature.

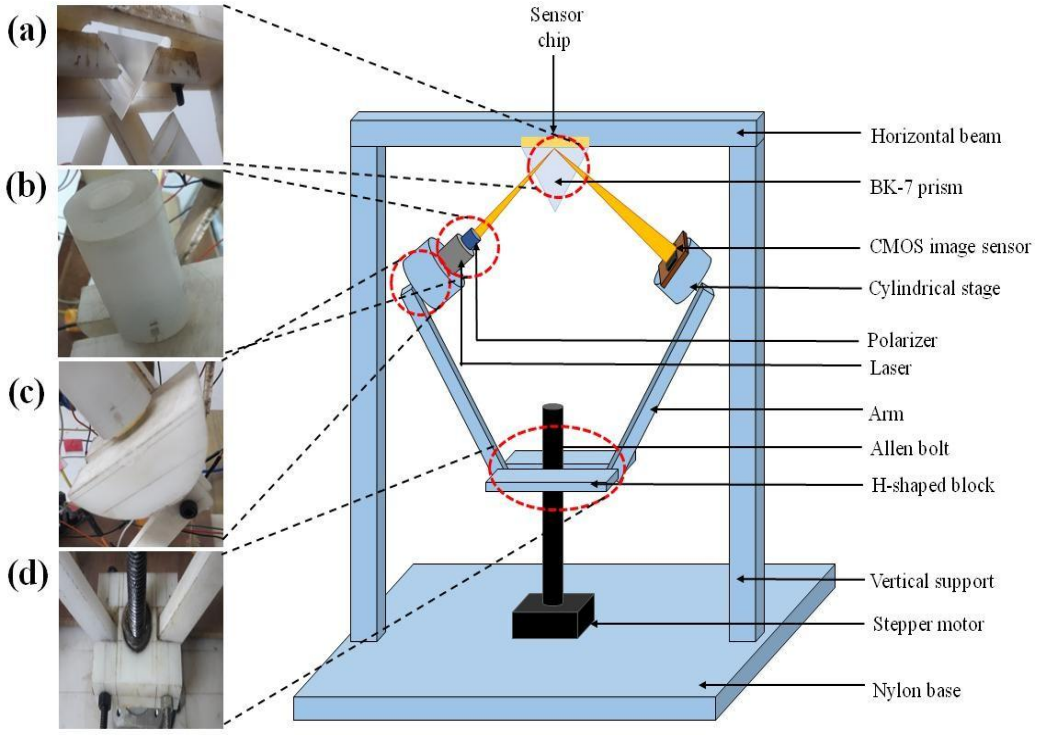

Figure 3.2: Schematic of the Portable SPR measurement prototype. Inset photographs show a) Removable mould for prism assembly b) Removable moulds for laser and detector (c) Two hemispherical stages (d) 'H-shaped' block

3.2.3 Fabrication of multiple protein-patterned SPR biosensors for detection of H-IgG

3.2.3.1 Multichannel microfluidic flow cell

Sylgard 184 was used for the fabrication of PDMS based microfluidic channels (length=20 mm, diameter=1.5mm) using a simple, fast and repeatable technique [29, 30]. The master mould for the fabrication of three channel PDMS polymeric replica was prepared using copper wires affixed to the metal plate. PDMS was fabricated using silicone elastomer and curing agent by mixing them thoroughly in a ratio of 10:1. The mixture was then placed in a vacuum chamber and desiccated for 10 min using a pump. After 10 min, when a significant number of bubbles appeared on the surface of the PDMS, the pump was turned off and the valve of the vacuum chamber was quickly pulled out to let the outside air in. The sudden difference in the pressure inside the chamber resulted in the elimination of most of the bubbles in the mixture. The valve was placed back and the pump was turned on to repeat the process until all the bubbles disappeared. The mixture was then directly poured over the master mould and allowed to cure in an oven at 100˚C for 1 h followed by cooling at room temperature for a period of 45 min. After the PDMS was cured completely, the copper wires were pulled out manually from the master mold leading to the formation of three cylindrical shaped microchannels on the PDMS flow cell measuring 20 mm in length and 1.5 mm in diameter. Six holes each measuring 1.5 mm in diameter were punched using a biopsy punch for the creation of separate inlets and outlets for each microchannel. The schematic representation of the PDMS casting process and multichannel microfluidic flow cell is shown in Figure 3.3(a, b).

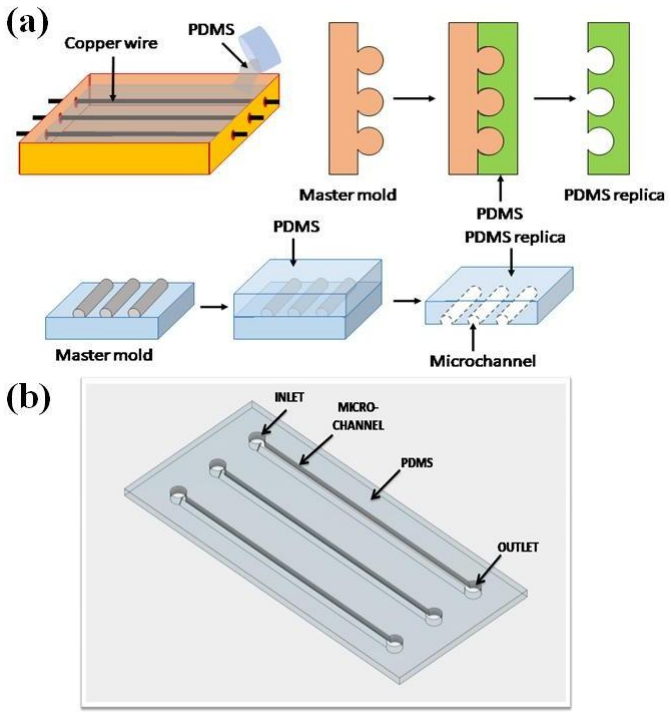

Figure 3.3: Schematic representation of a) PDMS casting process b) PDMS multichannel microfluidic flow cell

3.2.3.2 Sample preparation

Table 3.1 shows the specifications of the SPR biosensors fabricated in this research work with different concentrations of antibodies.

Polyclonal Antibodies: Lyophilized polyclonal antibodies of three varieties raised in mouse, goat and rabbit viz; M-aHIgG, G-aHIgG and R-aHIgG of different concentrations were prepared in PBS at pH of 7.4.

Antigen: Different concentrations of H-IgG antigen viz; ranging from 15-450 µg/ml were prepared in PBS.

Table 3.1: Specifications of the SPR Biosensors

Sample	Concentration of antibody(µg/ml)	Source of antibody
SPR Biosensor I	500	Mouse, goat and rabbit
SPR Biosensor II	750	Mouse, goat and rabbit
SPR Biosensor III	1000	Mouse, goat and rabbit

3.2.3.3 Multiple protein-patterned biosensor fabrication

For the fabrication of the multiple protein patterned SPR biosensors, BK7 glass substrates (50 mm x 26 mm x 1.25 mm, RI=1.51) were cleaned by sonicating in acetone, ethanol and DI water for 20 min each respectively. Sonication using acetone and ethanol was carried out to remove the organic contaminants on the substrates and sonication using DI water was used to remove the inorganic substances. Finally, the substrates were rinsed with DI water and dried. A layer of Titanium (Ti) (~5 nm) was then deposited on one side of the cleaned substrates using Radio Frequency (RF) magnetron sputtering technique at a deposition rate of 0.2 Å /sec followed by the deposition of Au (~50 nm) using Direct current (DC) magnetron sputtering at a deposition rate of 0.5 Å /sec to promote surface adhesion of Au film to glass. The RF and DC magnetron sputtered thin films were deposited using Argon (Ar) gas at the deposition pressure of $6x10^{-6}$ mbar at room temperature of 25˚C. Figure 3.4 shows the schematic diagram of the protocol used for bonding Au substrate with PDMS microfluidic chip for the fabrication of the multiple protein-patterned SPR biosensor. In the first process (Process I), the Au thin films [Figure 3.4a] were submerged in an acetone bath at 56°C to remove any organic residues arising from nanofabrication. Thereafter, the Au coated substrates were incubated for 24 h in a 5 mM ethanolic solution of 11-MUA for the formation of a Self-Assembled Monolayer (SAM). SAM comprises of thiol group which forms robust chemical bonds with Au required for the attachment of proteins on metal surfaces [Figure 3.4b]. The substrates were then cleaned with ethanol, dried and surface activated in a 1:1 mixture of 400 mM EDC and 100 mM NHS ethanolic solution for 1 h using amine coupling chemistry [Figure 3.4c]. In the second process (Process II), the PDMS microchannels (length=20 mm, diameter=1.5 mm) [Figure 3.4d] were immersed in 10% (v/v) ethanolic solution of 3- APTMS [Figure 3.4e] for 1 h followed by rinsing three times with ethanol and DI water. The surface activated Au substrates were then brought in contact with APTMS treated microfluidic flow cell. This novel bonding protocol ensures the irreversible and leakage-free bonding of PDMS microfluidic channels with Au substrates at room temperature [Figure 3.4f]. Polyclonal antibodies of different varieties and concentrations, as listed in Table 3.1, were injected separately through the individual inlet ports of the microchannels of the bonded SPR biosensor. The antibodies were immobilized over the Au substrates through the PDMS channels of the bonded chip for 1 h to develop a multiple protein-patterned SPR biosensor [Figure 3.4g]. 1M ethanolamine solution was passed through the microchannels of the SPR biosensors in order to prevent

undesired linking of the unreacted NHS esters and cleaning with PBS. Thereafter, the target antigen, H-IgG of varying concentrations was injected through the microchannels successively and exposed to different varieties of antibody proteins on the same SPR biosensor to study the interaction capacity.

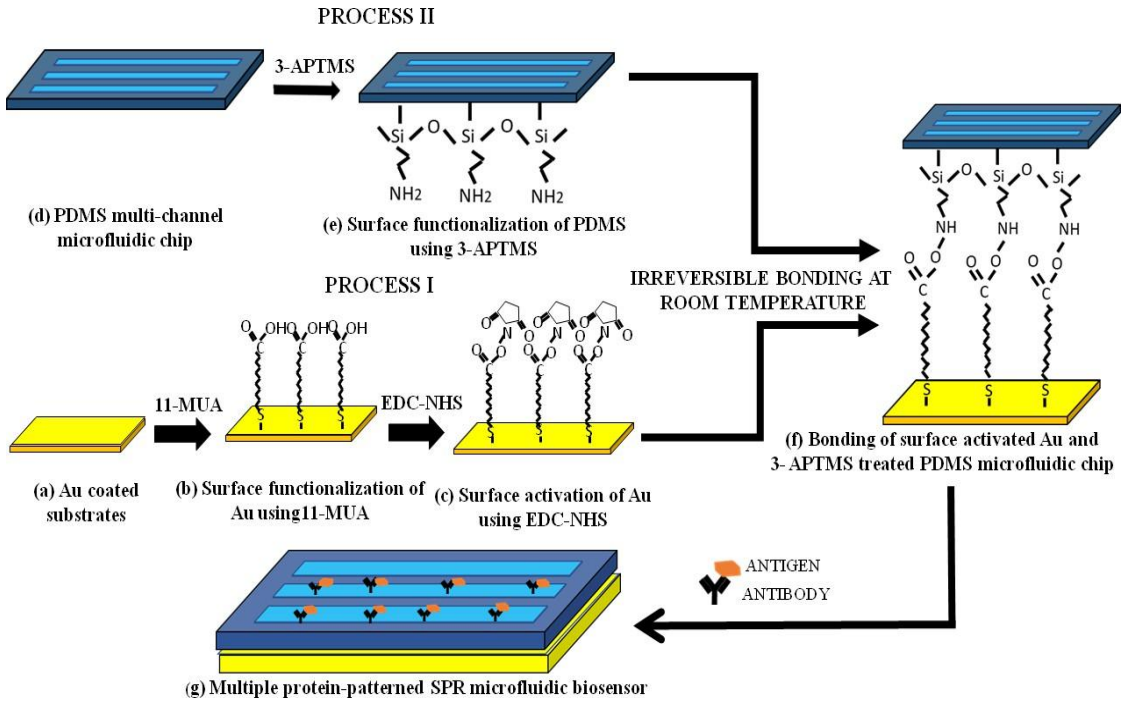

Figure 3.4: Schematic representation of the fabrication procedure of the multiple protein-patterned SPR biosensor

3.2.4 Fabrication of SPR biosensors for detection of crude snake venom

3.2.4. 1 Sample preparation

Polyvalent antivenom: Lyophilized polyvalent antivenom was reconstituted in water and dialysed with PBS at pH of 7.4 for a period of 24 h. Subsequently, the concentration was calculated using Nanodrop 2000 Spectrophotometer (Thermo Scientific, USA) and the final concentration was adjusted to 1000 ng/ml.

Venom: Different concentrations of crude *Naja naja* and *Daboia russelii* venom ranging from 10-1000 ng/ml were prepared in PBS. Shortly after envenomation and the onset of clinical symptoms, the concentration of the majority of snake venoms in serum or plasma was found to be more than 10 ng/ml; even exceeding 100 ng/mL to 1000 ng/ml in some

patients [31, 32]. The concentration range of the venom solutions was chosen to mimic the concentration of venoms in plasma after envenomation.

Platelet Poor Plasma (PPP): Fresh goat blood was collected in tubes containing 3.8% tri-sodium citrate (9:1, blood: tri-sodium citrate) for the preparation of plasma. Following a 20 min centrifugation at 900 g for the citrated blood, the yellowish supernatant containing PPP was pipetted out and used immediately [33].

3.2.4.2 Biosensor fabrication

Following the successful proof of concept with standard proteins, SPR biosensors were fabricated to study their interaction capacity towards different concentrations of *Naja naja* and *Daboia russelii* snake venoms. For the fabrication of the sensors, Au coated glass substrates were rinsed in ethanol and DI water after being incubated for 24 h in a 5 mM ethanolic solution of 11-MUA to generate a SAM. The SAM layers were surface activated by immersing the substrates in a 1:1 mixture of ethanolic solution of 400 mM EDC and 100 mM NHS for 1 h. Subsequently, the activated SAM layers were immobilized for 1 h by immersing them in a polyvalent antivenom solution followed by treatment with 1M ethanolamine to cap the unreacted NHS esters and cleaning with PBS. Thereafter, crude snake venoms of *Naja naja* and *Daboia russelii* of varying concentrations were exposed to the antivenom immobilized Au coated substrates successively and the SPR spectra were recorded.

3.2.5 Key performance parameters of SPR biosensors

The performance of the fabricated SPR biosensors was evaluated using some key performance parameters as listed below.

Sensitivity: The sensitivity of the SPR biosensor is expressed as the resonance angle shift (in ˚) per unit change in concentration (in μg/ml) of antigen solution [34].

LoD: The LOD of the SPR biosensor is expressed as the ratio of three times the standard deviation to the sensitivity [35].

Response time: The response time of the SPR biosensor is the amount of time needed for the SPR resonance angle to stabilize following the injection of antigen solution [34]. The response time is determined from the SPR sensorgrams which demonstrate the binding kinetics of the biomolecular interaction.

Selectivity: A critical parameter to evaluate the performance of a biosensor is its ability to respond selectively towards a target molecule. The selectivity of the SPR biosensor to respond selectively to a target protein is determined by measuring the response of the SPR biosensor towards various other protein molecules.

Repeatability and Reproducibility: The repeatability and reproducibility of the SPR biosensor are determined by comparing the resonance angle shifts for multiple measurements and biosensors respectively.

3.3 Results and Discussion

3.3.1 SPR response of standard samples and sensor characterization

The custom-made SPR prototype was tested using various standard samples of known RI. Figure 3.5 shows the variation of the SPR resonance angle with RI of air (RI=1), methanol (RI=1.3264) and water (RI=1.3317) for the bare ~50 nm coated Au film at a wavelength (λ) of 633 nm. It is observed from the figure that the resonant coupling of the Au film towards air, methanol and water resulted in a subsequent rise of resonance angle with an increase in RI of the sample.

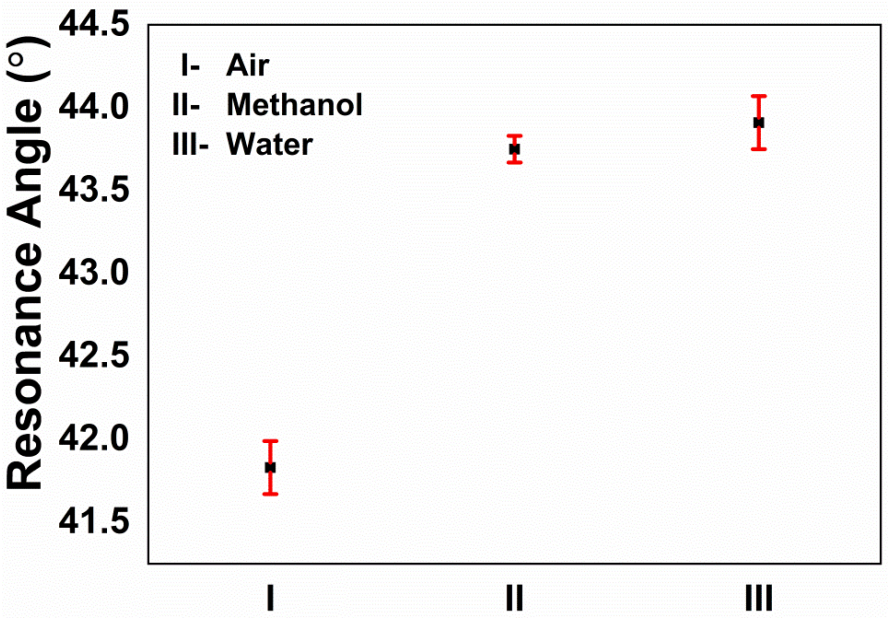

Figure 3.5: SPR response of a bare ~50 nm coated Au film towards air, methanol and water measured using the custom-made measurement prototype

The biosensor was characterized at each step of the fabrication process before the exposure to target antigen H-IgG using Ultraviolet-Visible (UV-Vis) absorption spectroscopy as illustrated in Figure 3.6. The absorbance peak for unmodified Au film occurred at ~520 nm. The absorbance peak shifted to ~527 nm after the functionalization of Au with 11-MUA. This resulted from the chemisorption of thiol molecules to the surface of Au. After functionalization, a shift to ~535 nm was noticed upon activation of the surface using EDC and NHS due to the formation of active NHS esters. A further shift to ~540 nm was observed due to the antibody conjugation with Anti-HIgG. The characteristic absorbance spectra and the subsequent redshift are similar to the results reported earlier [36-38]. The addition of multiple ligand layers to the Au surface results in successive rises in the local RI leading to redshift of the absorbance peak [39-41].

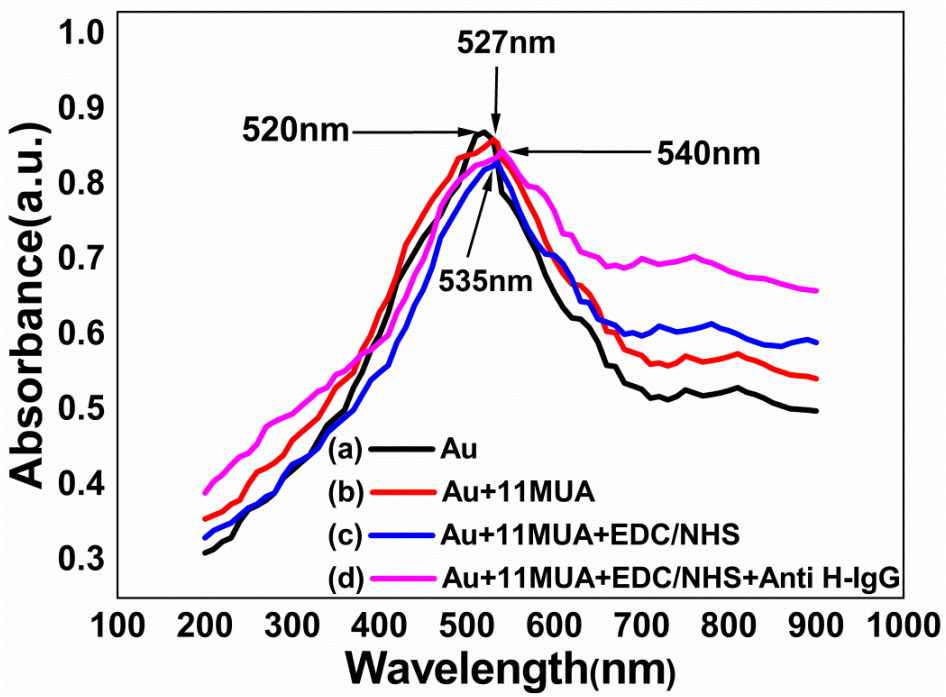

Figure 3.6: UV-Vis absorption spectra of SPR biosensor after each step of fabrication before exposure to target antigen H-IgG

3.3.2 Detection of H-IgG

3.3.2.1 SPR Response

Figure 3.7 presents the shift in the SPR resonance angle after each step of the fabrication process of SPR Biosensor I, SPR Biosensor II and SPR Biosensor III. The local RI increases with the functionalization of Au using 11-MUA followed by surface

activation with EDC-NHS and immobilization of polyclonal antibodies viz; M-aHIgG, G-aHIgG and R-aHIgG on SPR Biosensor I (Figure 3.7a), SPR Biosensor II (Figure 3.7b) and SPR Biosensor III (Figure 3.7c), resulting in redshift in SPR resonance. The changes in the RI are due to the growth of the SAM layer, conversion of the terminal groups present in the SAM layer into NHS active ester by EDC-NHS linking chemistry and immobilized antibodies on the activated SAM layer. The experimental results were repeated for multiple measurements and biosensors to confirm the repeatability and reproducibility of the antibody immobilization procedure.

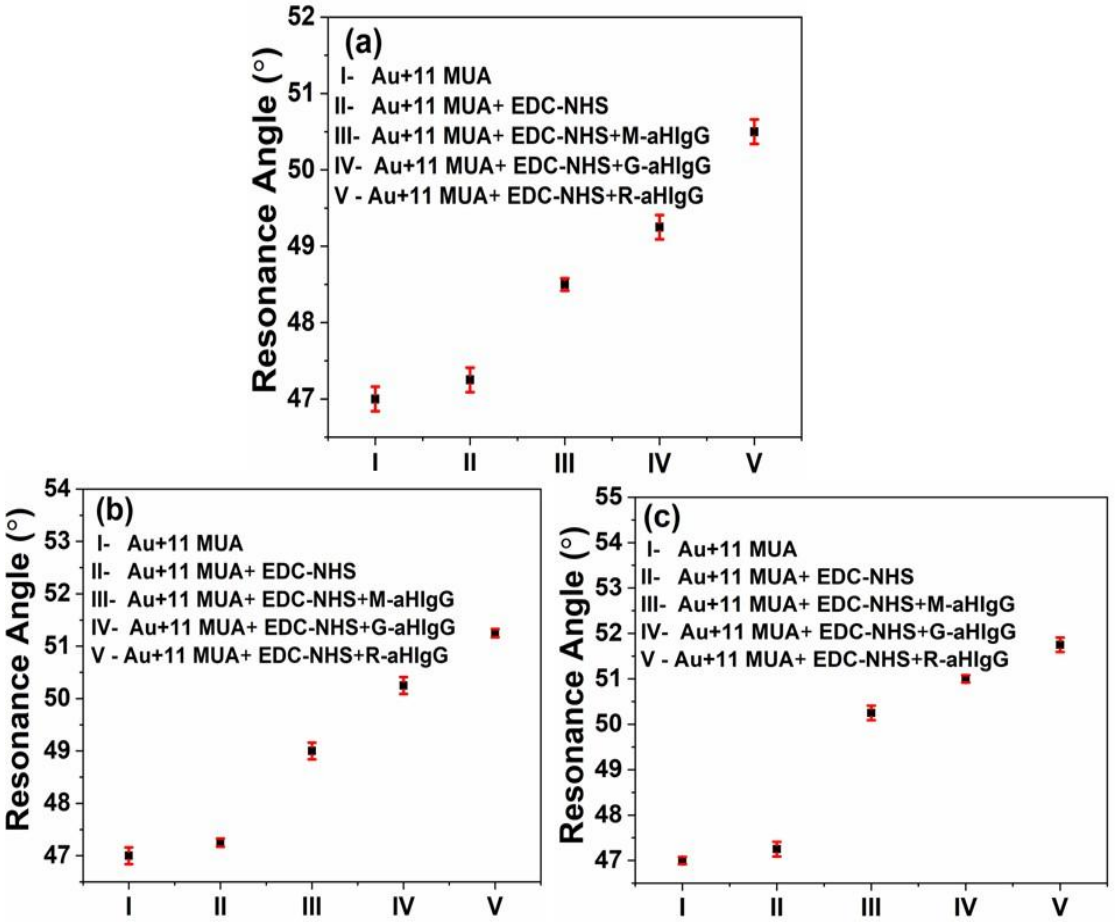

Figure 3.7: SPR response after each step of the fabrication process of (a) SPR Biosensor I, (b) SPR Biosensor II and (c) SPR Biosensor III

Figure 3.8 shows the variation in SPR resonance angle with increasing concentrations of H-IgG antigen (15 µg/ml-450 µg/ml) exposed to SPR Biosensor I, II and III. The binding of the H-IgG protein with the anti H-IgG resulted in local RI change near the sensor surface, resulting in corresponding shifts in resonance angles. For SPR Biosensor I, the interaction of H-IgG with the antibodies M-aHIgG, G-aHIgG and R-

aHIgG saturates at 240 µg/ml and the corresponding resonance angles are 68.5˚±0.25˚, 71.5˚±0.5˚ and 73.5˚±0.25˚ respectively (Figure 3.8a). It is interesting to observe that the sensor response is linear for a wide range of concentrations. The SPR Biosensor I produces linear response in the concentration range (45-240) µg/ml with R^2 values as 0.98800, 0.99198 and 0.99314 for M-aHIgG, G-aHIgG and R-aHIgG respectively (Figure 3.8b). Initially, an abundant number of active binding sites are present on the sensor surface which allows strong binding between H-IgG and anti H-IgG. The antigen-antibody binding results in a local RI change near the sensor surface which increases linearly with the increase in antigen concentration. Later as the binding kinetic progresses, a gradual decrease in the available active binding sites occurs, leading ultimately to a saturated sensor response. Similar results are obtained for SPR Biosensor II and III as depicted in Figure 3.8(c-f). The SPR Biosensor II and SPR Biosensor III exhibit linear response in the concentration range (15-225) µg/ml and (30-195) µg/ml respectively, beyond which the response of both the sensors saturate. The antigen, H-IgG is selective to all the three varieties of antibodies raised in mouse, goat and rabbit, however, the affinity and the degree of the interaction capacity varies with the type of antibody. This results in varying degrees of shifts in resonance angle on antigen-antibody interaction. In all the cases, the highest magnitude of resonance angle is observed for the interaction of R-aHIgG with H-IgG compared to M-aHIgG and G-aHIgG of the same concentration. This is due to the stronger interaction of H-IgG with R-aHIgG which could be attributed to the strong affinity of H-IgG to R-aHIgG over M-aHIgG and G-aHIgG. The sensitivities, linear range of detection, LoDs, saturation concentration and resonance angle at saturation of the SPR biosensors are determined from Figure 3.8 and a summary of the characteristics of the SPR biosensors is listed in Table 3.2. Overall, SPR Biosensor II exhibits the highest sensitivity (0.06663(˚/µg/ml), the lowest LoD (15 µg/ml) and the widest linear response with a concentration range (15 µg/ml -225 µg/ml) of H-IgG. Hence SPR Biosensor II was subsequently utilized for further studies. The LoDs of the SPR biosensors in this research work, are comparable to several recently reported works for the detection of protein using SPR [17, 18, 42]. However, the performance of PDMS microfluidics based SPR biosensors, such as sensitivities, LoDs etc. can be improved further by utilizing various surface modification techniques on PDMS like oxygen plasma treatment, Ultraviolet (UV)/ozone treatments etc. as well as the use of novel materials such as metal oxides, Two-Dimensional (2D) nanomaterials and their heterostructures etc.

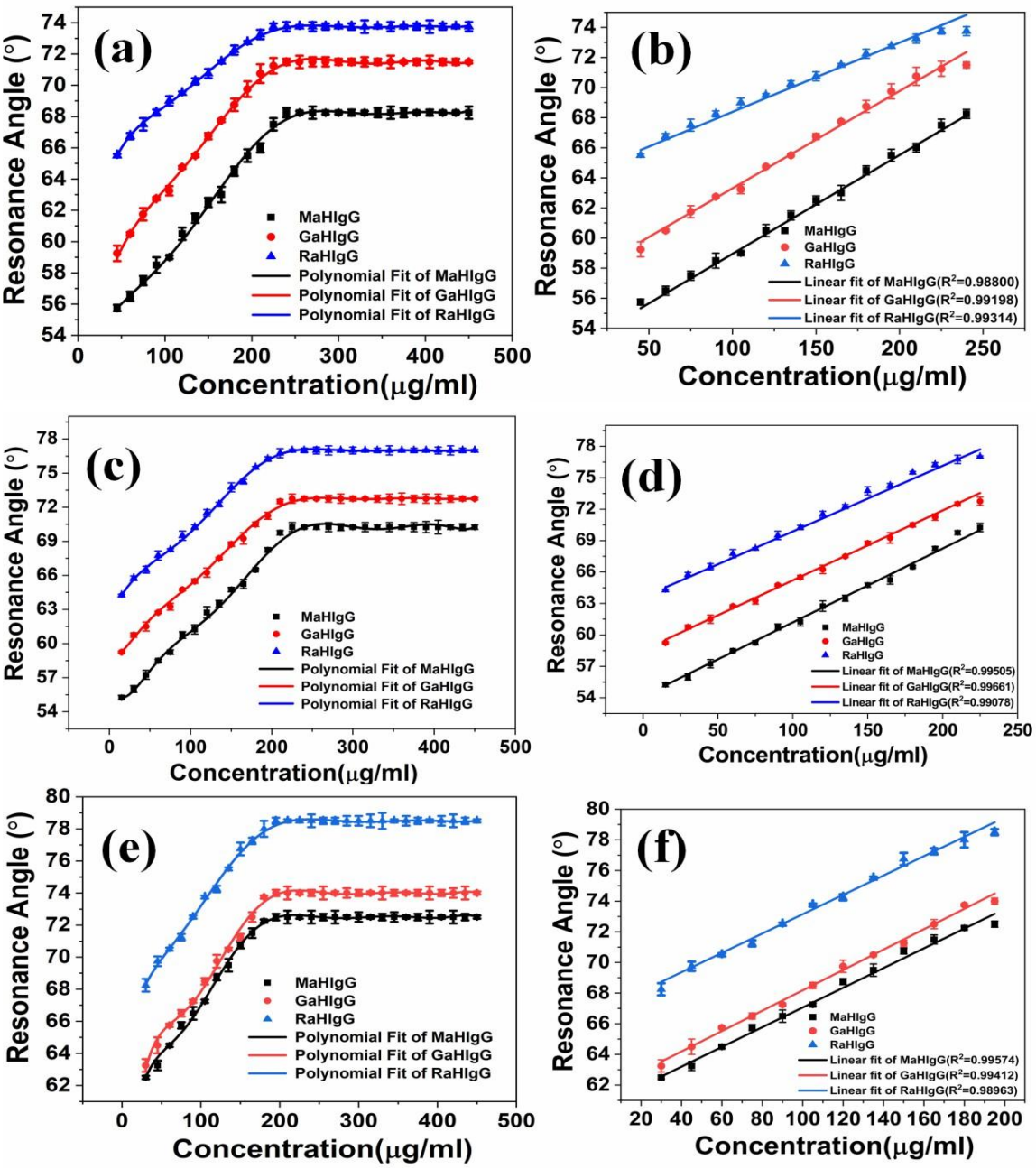

Figure 3.8: Variation in SPR angle with concentrations of H-IgG (15 μg/ml -450 μg/ml) exposed to (a-b) SPR Biosensor I (entire concentration range and linear fitted curve) (c-d) SPR Biosensor II (entire concentration range and linear fitted curve) (e-f) SPR Biosensor III (entire concentration range and linear fitted curve)

The sensitivity of the SPR biosensors can be practically determined by evaluating the slope of the graph showing the variation of the SPR dip shifts with the concentration of the antigen exposed to the biosensor. Hence the sensitivities of the SPR Biosensor I, SPR Biosensor II and SPR Biosensor III are evaluated by determining the slopes of the graphs showing the variation of the SPR resonance angle with the concentration of H-IgG.

Table 3.2: Summary of the characteristics of the SPR biosensors

Biosensor	Antibody	Saturation Concentration (µg/ml)	Resonance angle at saturation	Linear range of detection (µg/ml)	Sensitivity (˚/µg/ml)	R^2
SPR Biosensor I	M-aHIgG	240	68.5˚±0.25˚	45-240	0.05882	0.98800
	G-aHIgG		71.5˚±0.5˚			0.99198
	R-aHIgG		73.5˚±0.25˚			0.99314
SPR Biosensor II	M-aHIgG	225	70.25˚±0.5˚	15-225	0.06663	0.99505
	G-aHIgG		72.75˚±0.25˚			0.99661
	R-aHIgG		77˚±0.25˚			0.99078
SPR Biosensor III	M-aHIgG	195	72.5˚±0.75˚	30-195	0.06463	0.99574
	G-aHIgG		74˚±0.25˚			0.99412
	R-aHIgG		78.5˚±0.5˚			0.98963

3.3.2.2 Binding Kinetics

Figure 3.9 shows the SPR sensorgrams demonstrating the binding kinetics due to the biomolecular interaction of the H-IgG antigen (225 µg/ml) with SPR Biosensor II illustrating the association phase (insertion of H-IgG antigen) and dissociation phase (replacement of antigen with PBS). Initially, a baseline measurement was established by injecting PBS over the sensor chip for 5 min. As H-IgG is introduced, the association of the protein causes the resonance angle to rise subsequently reaching a steady state value. It is observed from Figure 3.9(a-c) that the sensor response saturates in around 10-15 min for M-aHIgG, G-aHIgG, R-aHIgG. Thereafter, the substitution of the H-IgG antigen with PBS results in the dissociation of protein from the sensor surface resulting in the resonance angle returning close to the baseline value. It is observed from the figure that the dissociation of H-IgG protein initiates earliest for M-aHIgG (~21 min) followed by G-aHIgG (~23 min) and R-aHIgG (~25 min). This is because of the fact that highly associated R-aHIgG protein on the sensor surface requires more time to dissociate, as compared to G-aHIgG and M-aHIgG. The obtained results are comparable to that reported by Tokel *et.al.* [20] and Li. *et.al.* [42].

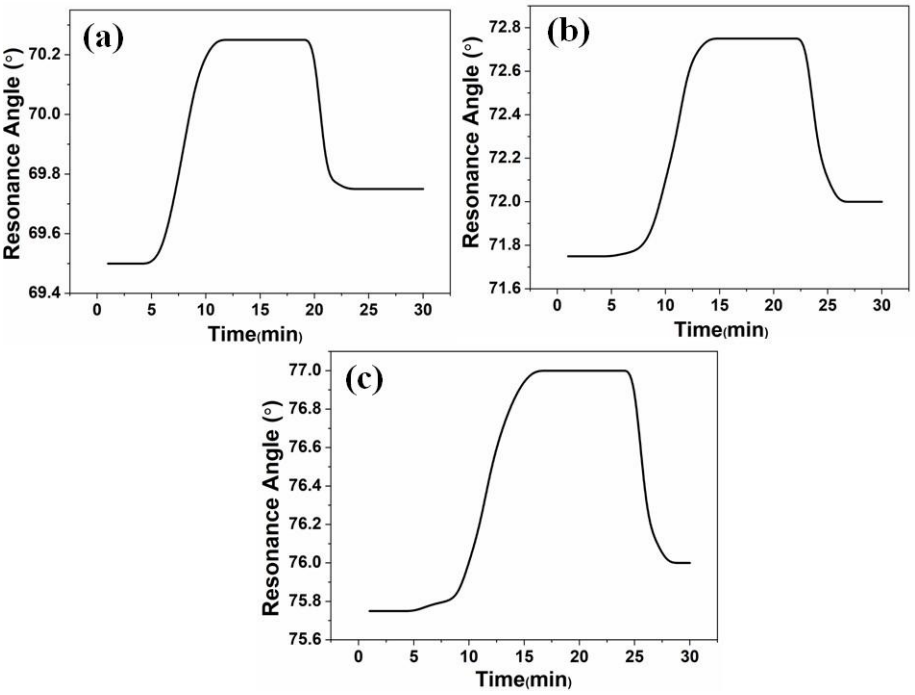

Figure 3.9: SPR sensorgrams showing the binding kinetics of H-IgG antigen (225µg/ml) with SPR Biosensor II for a) M-aHIgG b) G-aHIgG c) R-aHIgG

3.3.2.3 Selectivity

The feasibility of the biosensor to respond selectively to H-IgG was determined by measuring the response of SPR Biosensor II towards various other protein molecules like Bovine Serum Albumin (BSA) and Polyvalent Antivenom. The selectivity was determined by measuring the maximum resonance shift exhibited by SPR Biosensor II following exposure to two different concentrations viz, 15 µg/ml and 30 µg/ml, of target antigen and the results are presented in Figure 3.10. It is observed from Figure 3.10a that M-aHIgG produces a resonance angle shift of 0.25˚ and 0.75˚ against H-IgG of concentration 15 µg/ml and 30 µg/ml respectively, whereas the non specific targets (BSA and Antivenom) exhibit negligible resonance shift. Similarly, G-aHIgG (Figure 3.10b) demonstrates a significantly high resonance shift of 1.25˚ and 1.5˚ for 15 µg/ml and 30 µg/ml of H-IgG, respectively, whereas BSA and Antivenom protein show very small resonance shifts. Similarly, for R-aHIgG (Figure 3.10c), BSA and Antivenom show negligible resonance shifts while in comparison H-IgG shows significantly high shifts of 1.25˚ and 1.5˚ for 15 µg/ml and 30 µg/ml respectively. The measured data thus indicates that the sensor is selective to only H-IgG with negligible SPR signals towards BSA and Antivenom protein.

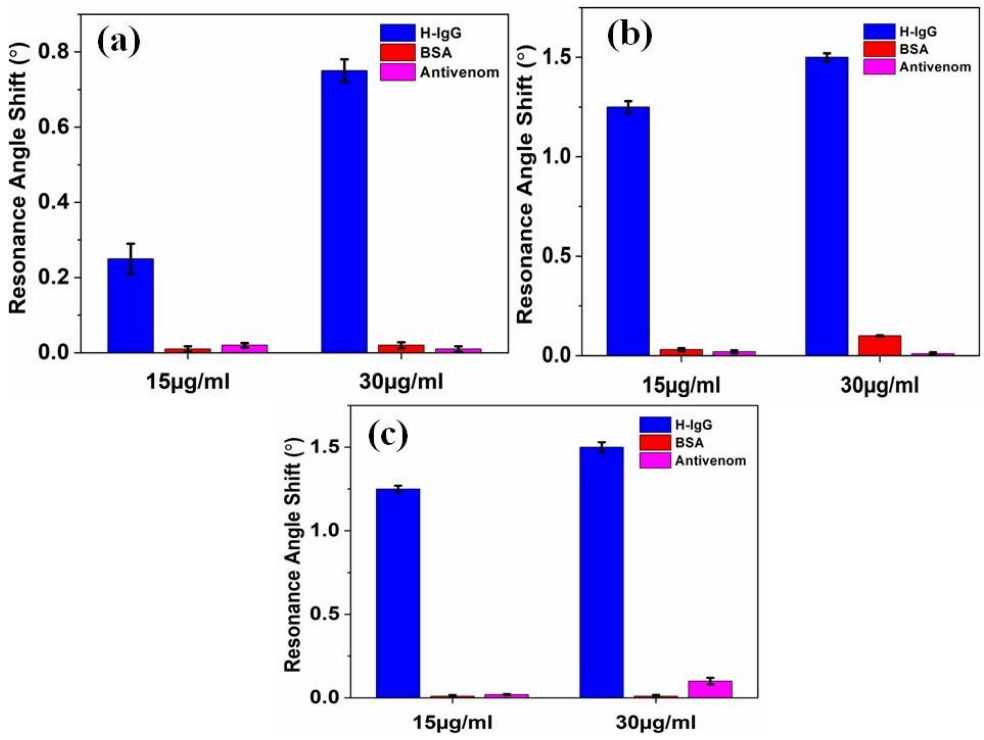

Figure 3.10**:** Selective response of the SPR biosensor II towards H-IgG, BSA and Antivenom for a) M-aHIgG b) G-aHIgG and c) R-aHIgG

3.3.3 Detection of crude snake venoms

3.3.3.1 SPR Response

Figure 3.11a illustrates the SPR response showing the variation in resonance angle after each process step in biosensor fabrication. The successive deposition and bonding among various stacked layers, viz., 11-MUA, EDC-NHS and the polyvalent antivenom on the sensor surface results in subsequent shifts in the resonance angle due to the rise in the effective RI as observed in the figure. Figure 3.11(b-c) shows the variation in SPR resonance angle with concentrations of *Naja naja* and *Daboia russelii* venoms exposed to the biosensor. The binding of the snake venom antigen to the antivenom produces an effective increment in the RI near the sensing surface manifested as a change in the SPR resonance angle. A strong interaction between the venom protein and antivenom occurs due to the initial abundance of active binding sites on the antivenom, resulting in a change in local RI at the sensor surface, producing a linear rise of SPR resonance angle with increment in concentration of antigen in the range 10-900 ng/ml (R^2=0.99) [inset of Figure 3.11(b-c)]. Later with further progress in the binding kinetics, a gradual decrease of the active binding sites causes the response of the sensor to saturate

beyond 900 ng/ml. The sensitivities and LoDs of the SPR biosensor are evaluated from Figure 3.11(b-c). The values of the sensitivities were determined to be 9.01678 (˚/µg/ml) and 10.32268 (˚/µg/ml) while the LoDs values were evaluated to be 9.37 ng/ml and 9.89 ng/ml for *Naja naja* and *Daboia russelii* respectively. The difference in the sensitivities and the LoD for the two varieties of snake venoms is attributed to the difference in the composition of their constituent proteins. The LoD of the biosensor, in this work, is comparable to several recently reported works for the detection of snake venom based on different techniques [43-45].

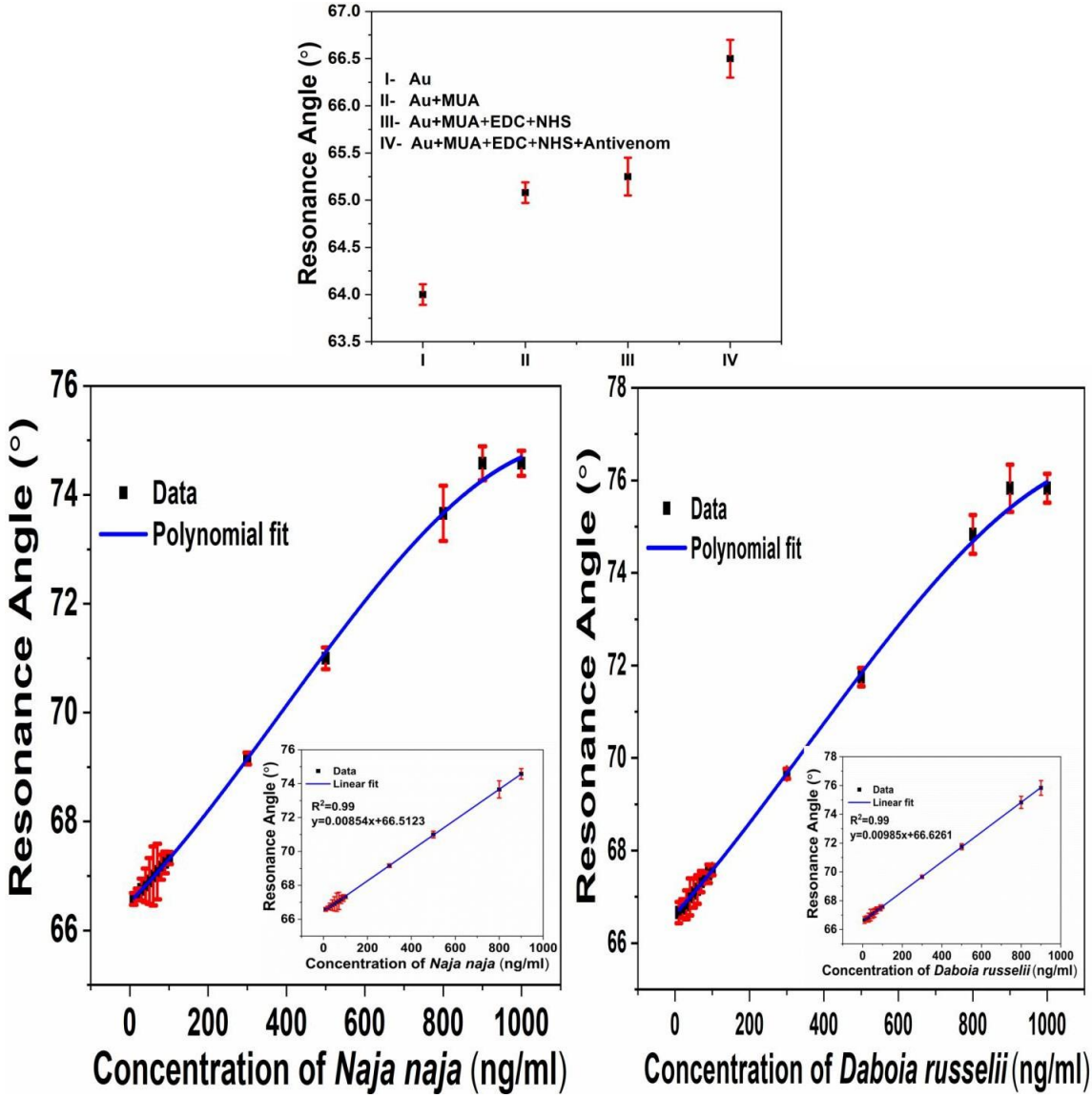

Figure 3.11: (a) SPR response after each step of the biosensor fabrication (b-c) Variation of SPR resonance angle with different concentrations of *Naja naja* and *Daboia russelii* venoms exposed to the biosensor respectively

3.3.3.2 Binding Kinetics

Figure 3.12 shows the SPR sensorgrams demonstrating the binding kinetics of the *Naja naja* venom of different dozes with the antivenom illustrating the association phase (insertion of venom antigen) and the dissociation phase (substituting venom antigen with PBS). It is observed from the figure that, with the introduction of each dose of the snake venom solution, the SPR resonance angle rises slowly to a steady state value due to the binding between the snake venom protein and the antivenom, saturating in around 16-17 min. Thereafter, PBS is injected into the sensor surface to cause the venom antigen to dissociate from the antivenom which causes the resonance angle to nearly revert to its initial position.

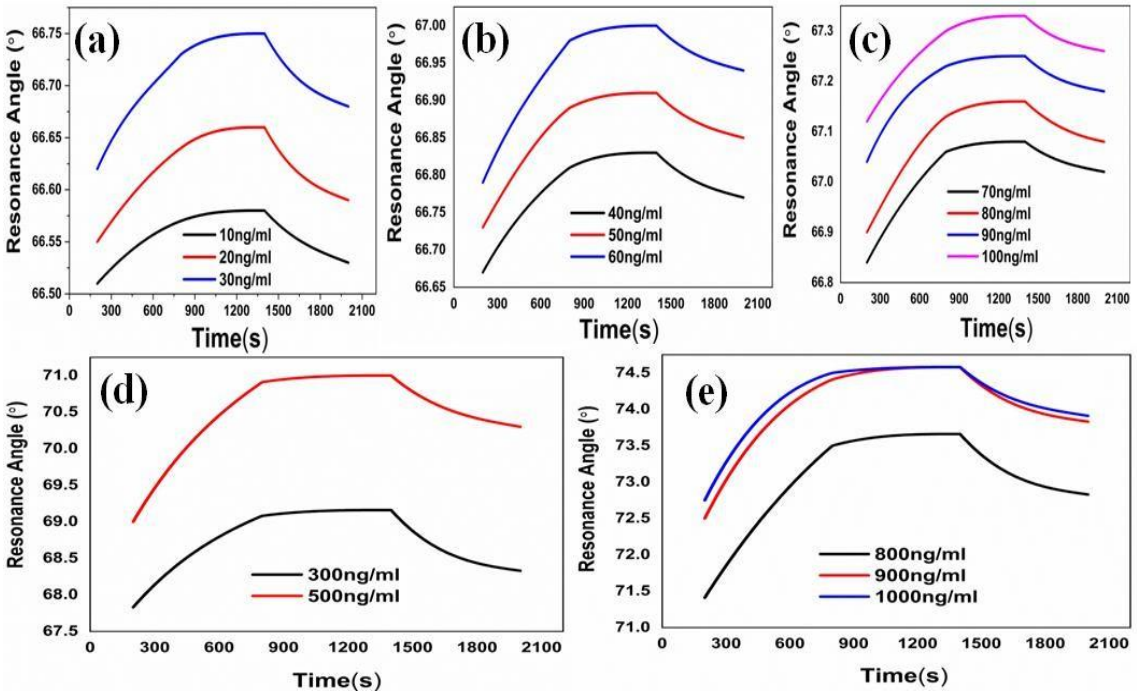

Figure 3.12: SPR sensorgrams showing the binding kinetics of *Naja naja* venom solution of varying concentrations (a) 10-30 ng/ml (b) 40-60 ng/ml (c) 70-100 ng/ml (d) 300-500 ng/ml (e) 800-1000 ng/ml

Figure 3.13 shows the SPR sensorgrams depicting the binding kinetics of the *Daboia russelii* venom solution of different concentrations with the antivenom illustrating the association phase and the dissociation phase. Similar to the *Naja naja* venom, with the introduction of each concentration of *Daboia russelii* venom solution, the association of the venom antigen with the antivenom leads to a gradual increase of the resonance angle achieving a steady state after around 20 min. The dissociation of the

venom antigen from the antivenom, with the introduction of PBS, results in the resonance angle returning close to the initial value. The difference in the response time of both the venom proteins is attributed to the difference in the composition of their constituent proteins affecting their binding interaction with the polyvalent antivenom. The response time of 16-20 min of the SPR biosensor for both the venoms, *Naja naja* and *Daboia russelii*, shows that the SPR based approach presents a much faster platform for snake venom detection compared to commercial methods like PCR, ELISA etc. which require a longer time of the order of few hours to produce results.

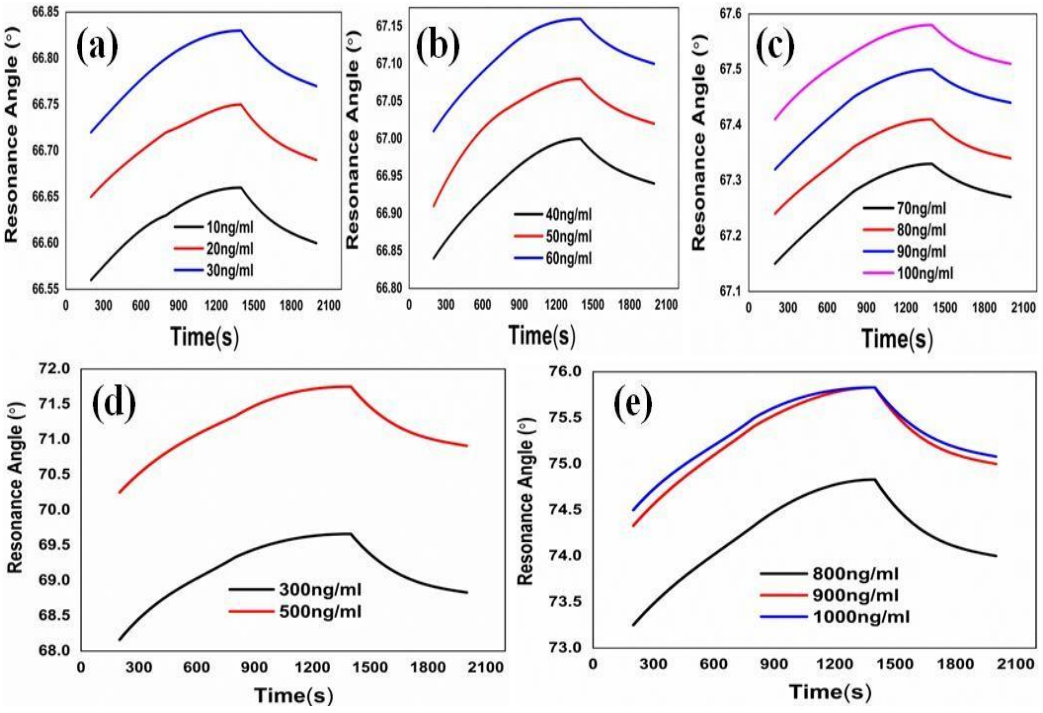

Figure 3.13: SPR sensorgrams showing the binding kinetics of *Daboia russelii* venom solution of varying concentrations (a) 10-30 ng/ml (b) 40-60 ng/ml (c) 70-100 ng/ml (d) 300-500 ng/ml (e) 800-1000 ng/ml

3.3.3.3 Repeatability and Reproducibility

The repeatability of the SPR biosensor was determined by comparing the resonance angle shifts for seven sets of measurements as shown in Figure 3.14(a-b). The sensor was exposed to every concentration of snake venom solution starting from 10 ng/ml to 1000 ng/ml in a sequential manner. The standard deviation and variance of the seven sets of measurements of *Naja naja* venom are evaluated to be 0.08180 and 0.0067 respectively. Similarly, the standard deviation and variance of the seven sets of

measurements of *Daboia russelii* venom are obtained as 0.07108 and 0.0050 respectively. The reproducibility of the sensor was also investigated by comparing the resonance angle shifts for seven sets of sensors as illustrated in Figure 3.14(c-d). Each sensor was exposed to every concentration of snake venom solution starting from 10 ng/ml to 1000 ng/ml in a sequential manner. The standard deviation and variance of the measurements for the seven sets of sensors for *Naja naja* venom are evaluated to be 0.109 and 0.011 respectively. Similarly, the standard deviation and variance of the measurements for *Daboia russelii* venom are obtained as 0.120 and 0.014 respectively. These results show a highly satisfactory repeatable and reproducible response of the SPR biosensor to detect crude snake venoms.

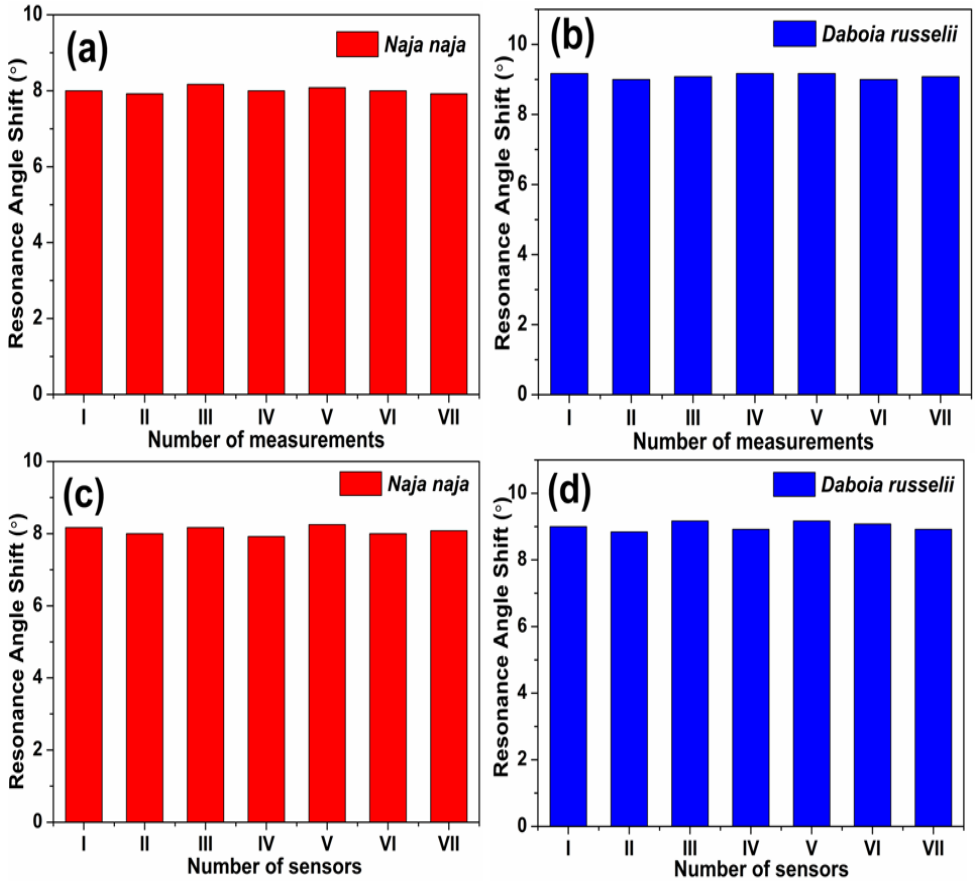

Figure 3.14: (a-b) Repeatability and (c-d) Reproducibility of the SPR biosensor to detect *Naja naja* and *Daboia russelii* venoms respectively

3.3.3.4 Stability

The stability of the sensor is a crucial parameter that determines its robustness. The stability of the SPR biosensors was evaluated by exposing them to every concentration of snake venom solutions (*Naja naja* and *Daboia russelii*) starting from 10 ng/ml to 1000 ng/ml in a sequential manner and examining their sensing response every week. Each of the three sets of sensors was exposed to the venom solutions every week followed by washing with PBS and storing in at 4°C. Table 3.3 shows the sensing response (resonance angle shifts) of the SPR biosensors towards *Naja naja* and *Daboia russelii* venoms for four cycles of experiments (4 weeks). It is observed from the table that after every cycle of the experiment, there is a decreasing trend of the resonance angle shift, indicating marginal degradation of the sensing performance of the SPR biosensor. After 4 cycles of repetitions, there is a ~3% decrement of resonance angle shift from the 1st cycle, both for *Naja naja* and *Daboia russelii* venoms which indicates a good stability of the sensor, supporting their suitability for field deployment. Besides the sensing material layer (snake venom antigen), the crosslinker layer (SAM and ECH/NHS) and the receptor (antivenom), the stable, repeatable and reproducible performance of the SPR biosensor is substantially dictated by the durability of the Au film on the substrates.

Table 3.3: Stability of the SPR biosensors

Crude venom	Biosensor No.	Cycle No (Approx. time)	Resonance angle shift (°)	Percentage degraded
Naja naja	I	Week 1	8	---
		Week 2	7.92	1%
		Week 3	7.83	2.12%
		Week 4	7.75	3.12%
	II	Week 1	8.08	---
		Week 2	8	0.99
		Week 3	7.92	1.98%
		Week 4	7.83	3.09%
	III	Week 1	7.92	---
		Week 2	7.83	1.13%
		Week 3	7.75	2.14%
		Week 4	7.67	3.16%
Daboia russelii	I	Week 1	9.17	---
		Week 2	9.09	0.98%
		Week 3	9	1.85%
		Week 4	8.92	2.73%
	II	Week 1	9	---
		Week 2	8.91	1%
		Week 3	8.84	1.77%
		Week 4	8.75	2.77%
	III	Week 1	9.09	---
		Week 2	9	1%
		Week 3	8.91	1.98%
		Week 4	8.84	2.75%

3.3.3.5 Control experiment and selectivity

The control experiments were conducted to determine the effectiveness of the immobilized antivenom and the non-specificity of the other layers. Figure 3.15a illustrates the SPR response of different layers on the substrate when exposed to the crude venom protein of concentrations 10 ng/ml and 1000 ng/ml. In these measurements, the baseline is established by exposing the sensor to 10 ng/ml venom solution first and then the shift in the resonance angle is noted when the sensor is exposed to 1000 ng/ml of the antigen solution. It is evident from the figure that bare Au film produces a negligible SPR shift. The direct attachment of antivenom on the Au film also does not produce a prominent resonance shift. Similar results are also obtained for substrates with the addition of SAM layer on Au film using 11-MUA and activation with EDC-NHS. The negligible response is due to the ineffective adsorption of venom protein on the sensor surface. The maximum response is only observed after the immobilization of the antivenom ligand on the sensor surface. The strong affinity of the antivenom immobilized on the sensor surface towards the venom protein changes the RI of the medium resulting in a large shift in the SPR dip.

The feasibility of the sensor to respond selectively to crude snake venom protein was determined by evaluating its response towards various other non-target protein molecules like BSA and H-IgG, which are present in real blood plasma and may interfere during snake venom antigen detection. The use of BSA and H-IgG protein for the selectivity test is justified because albumins and immunoglobulins are the most abundant proteins in blood plasma. The selectivity of the sensor was determined by exposing the sensor to BSA, H-IgG, *Naja naja* venom and *Daboia russelii* venom solutions in the range (10- 1000) ng/ml and comparing the resonance angle shifts as illustrated in Figure 3.15b. The figure clearly illustrates the insignificant response of the SPR biosensor towards the other biomolecules in comparison to *Naja naja* and *Daboia russelii* venoms. This negligible response of the sensor towards other proteins results from the selective interaction of the venom protein with the polyvalent antivenom immobilized on the surface of the sensor for specific binding chemistry. Therefore, the SPR biosensor can be used to detect crude snake venom antigens in real blood plasma samples due to its selectivity.

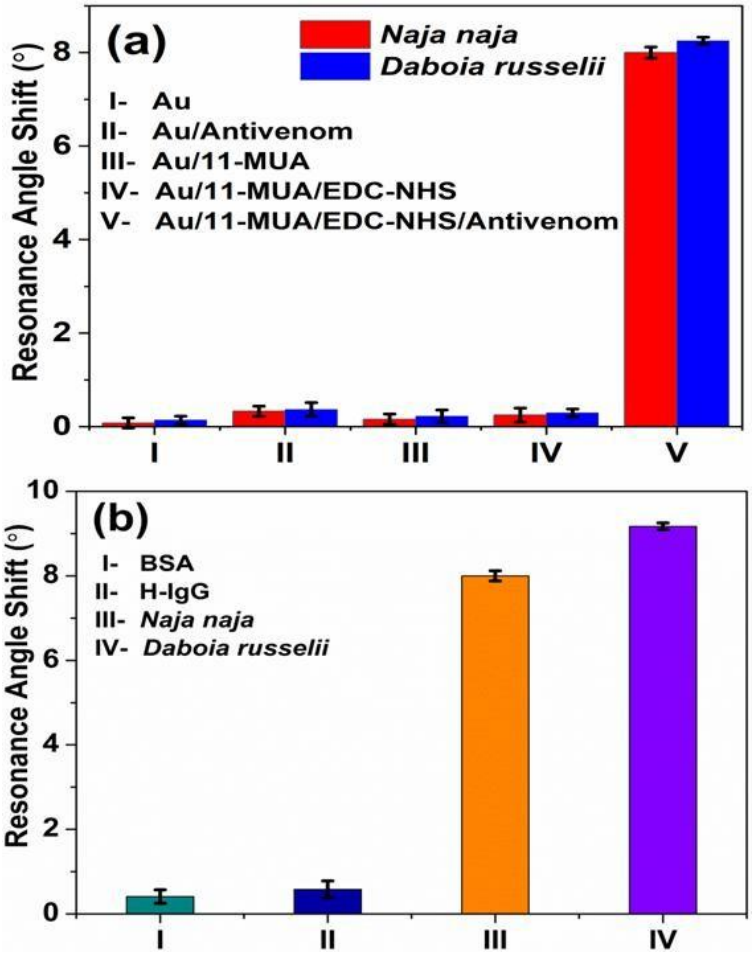

Figure 3.15: (a) Control experiment to determine the effectiveness of the immobilized antivenom and the non-specificity of the other layers (b) Selectivity of the SPR biosensor towards BSA, H-IgG, *Naja naja* venom and *Daboia russelii* venom

3.3.3.6. Real sample analysis

The feasibility of the present approach was determined by testing the crude snake venoms in real blood plasma samples. The SPR sensors were exposed to every concentration of *Naja naja* and *Daboia russelii* venom, prepared in blood plasma, starting from 10 ng/ml to 1000 ng/ml in a sequential manner and the results are presented in Figure 3.16. The figure shows that the resonance angle increases with increasing doses of *Naja naja* and *Daboia russelii* venoms diluted in blood plasma samples, producing a linear range of 10-900 ng/ml (R^2=0.98). The results closely align with the ones evaluated for artificial crude snake venom samples (prepared in PBS) which successfully demonstrates the feasibility of the SPR biosensor and plasmonic biosensing platform for sensing in non-ideal and practical conditions.

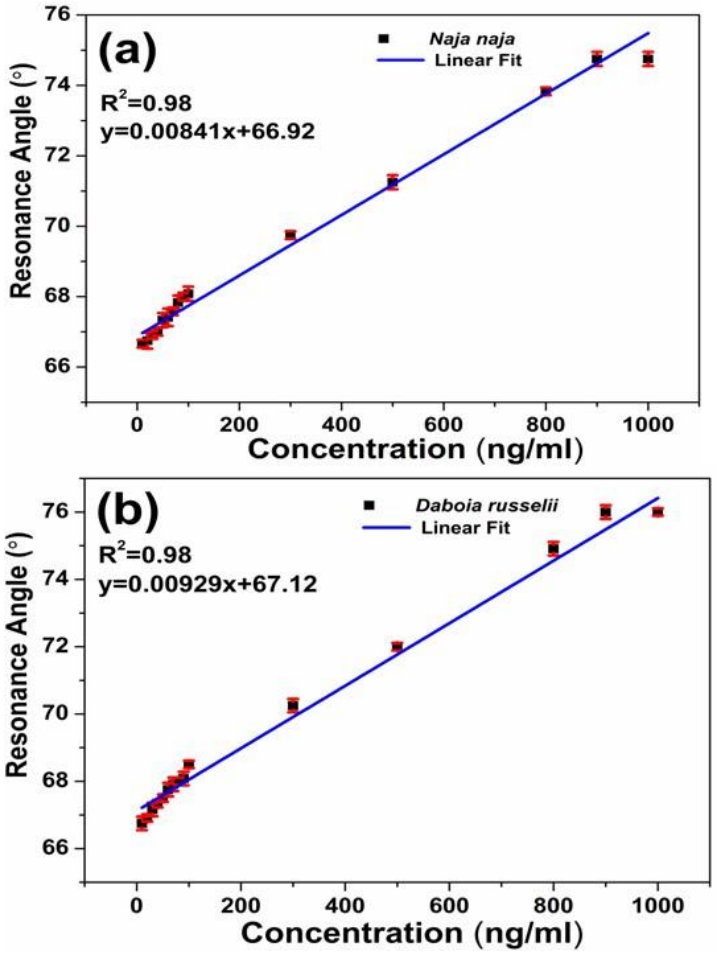

Figure 3.16: SPR response towards varying dilutions of crude snake venoms in blood plasma samples for (a) *Naja naja* and (b) *Daboia russelii*

3.3 Summary

This chapter presents the construction of SPR biosensors patterned with multiple proteins fabricated using a novel bonding protocol to ensure the bonding of PDMS microchannels (length=20 mm, diameter = 1.5 mm) with Au substrates. The novelty of the bonding protocol lies in the irreversible bonding of PDMS microfluidic channels with gold substrates at room temperature ensuring leakage-free channels. Polyclonal antibodies viz; M-aHIgG, G- aHIgG and R-aHIgG were immobilized through the microchannels over the surface activated Au substrates and exposed to a target antigen protein, H-IgG to study the interaction capacity of the biosensors. The H-IgG antigen was selective to all three varieties of antibodies, however, the affinity and the degree of the interaction capacity varied with the type of antibody. The SPR Biosensor II exhibited the highest average sensitivity (0.06663(˚/µg/ml), lowest LoD (15 µg/ml), wide linear response (15 µg/ml- 225 µg/ml) with a response time of ~12 min exhibiting selective detection of H-IgG with negligible response towards other interfering proteins like BSA and Polyvalent Antivenom.

A custom-made, robust and miniaturized SPR measurement prototype was fabricated in the Kretschmann configuration to perform the sensing study. Robust construction was emphasized in order to eliminate vibrational errors, misalignment of optical components etc. The prototype, measuring 300 mm x 250 mm x 250 mm and weighing ~3.5 kg, was driven by a single stepper-motor to ensure synchronous movement of the light source (633 nm) and the detector (CMOS linear image sensor, 512 pixel) for SPR measurement. Following the successful proof of concept with standard proteins, SPR biosensors were fabricated by immobilizing polyvalent antivenom for the detection of *Naja naja* and *Daboia russelii* snake venoms of different concentrations. The SPR biosensors offered a wide linear range (10 ng/ml-900 ng/ml, R^2=0.99), providing a sensitivity of 9.01678˚/(µg/ml) for *Naja naja* venom and 10.32268˚/(µg/ml) for *Daboia russelii* venom with LoD of 9.37 ng/ml for *Naja naja* venom and 9.89 ng/ml for *Daboia russelii* venom. Besides, the biosensors showed a response time of ~16-20 min producing repeatable, reproducible and stable results. The SPR biosensors selectively interacted with the snake venom proteins showing negligible response towards other interfering proteins like BSA and H- IgG. Further, the satisfactory response of the SPR biosensors with snake venoms in real blood plasma samples establishes their feasibility for practical applications.

Bibliography

[1] Wang, D. S., & Fan, S. K. Microfluidic surface plasmon resonance sensors: From principles to point-of-care applications. *Sensors*, 16(8): 1175, 2016.

[2] Bakouche, M. T., Ganesan, S., Guérin, D., Hourlier, D., Bouazaoui, M., Vilcot, J. P., & Maricot, S. Leak-free integrated microfluidic channel fabrication for surface plasmon resonance applications. *Journal of Micromechanics and Microengineering*, 30(12): 125003, 2020.

[3] Amreen, K., Salve, M., & Goel, S. Portable Electrochemical Platform With Carbon Fibre Microelectrodes Integrated on an OHP Sheet for Snake Venom Analysis. *IEEE Transactions on NanoBioscience*, 22(1): 149-154, 2022.

[4] Coulter, A. R., Sutherland, S. K., & Broad, A. J. Assay of snake venoms in tissue fluids. *Journal of Immunological Methods*, 4(2): 297-300, 1974.

[5] Kabir, M. A., Zilouchian, H., Younas, M. A., & Asghar, W. Dengue detection: advances in diagnostic tools from conventional technology to point of care. *Biosensors*, 11(7): 206, 2021.

[6] Cooper Jr, J. A., Mintz, B. R., Palumbo, S. L., & Li, W. J. Assays for determining cell differentiation in biomaterials. *Characterization of Biomaterials; Jaffe M., Hammond W., Tolias P., Arinzeh T. (Eds.); Woodhead Publishing: Sawston, United Kingdom*: 101-137, 2013.

[7] Kumbhat, S., Sharma, K., Gehlot, R., Solanki, A., & Joshi, V. Surface plasmon resonance based immunosensor for serological diagnosis of dengue virus infection. *Journal of Pharmaceutical and Biomedical Analysis*, 52(2): 255-259, 2010.

[8] Feng, C. Q., Tang, X. J., Huang, L. Q., Qian, Z. Z., Zhang, J., & Cui, G. H. High specific PCR identification of Bungarus multicinctus and its adulterants. *China Journal of Chinese Materia Medica*, 31(13): 1050-1053, 2006.

[9] Dubey, B., Meganathan, P. R., & Haque, I. Molecular identification of three Indian snake species using simple PCR–RFLP method. *Journal of forensic sciences*, 55(4): 1065-1067, 2010.

[10] Lo, S. J., Yang, S. C., Yao, D. J., Chen, J. H., Tu, W. C., & Cheng, C. M. Molecular-level dengue fever diagnostic devices made out of paper. *Lab on a Chip*, 13(14): 2686-2692, 2013.

[11] Ngo, H. T., Wang, H. N., Fales, A. M., Nicholson, B. P., Woods, C. W., & Vo-Dinh, T. DNA bioassay-on-chip using SERS detection for dengue diagnosis. *Analyst*, 139(22): 5655-5659, 2014.

[12] Cheng, Y., Ye, X., Ma, Z., Xie, S. & Wang, W. High-throughput and clogging-free microfluidic filtration platform for on-chip cell separation from undiluted whole blood. *Biomicrofluidics*, 10:014118, 2016.

[13] Mark, D., Haeberle, S., Roth, G., Von Stetten, F. & Zengerle, R. Microfluidic lab-on-a-chip platforms: requirements, characteristics and applications. *Chem. Soc. Rev*., 39:1153–1182, 2010.

[14] Hassani, A. & Skorobogatiy, M. Design of the microstructured optical fiber-based surface plasmon resonance sensors with enhanced microfluidics. *Optics Express*, 14:11616–11621, 2006.

[15] Brown, X.Q., Ookawa, K. & Wong, J.Y. Evaluation of polydi- methylsiloxane scaffolds with physiologically-relevant elastic moduli: Interplay of substrate mechanics and surface chemistry effects on vascular smooth muscle cell response. *Biomaterials*, 26:3123–3129, 2005.

[16] Eroshenko, N., Ramachandran, R., Yadavalli, V.K. & Rao, R.R. Effect of substrate stiffness on early human embryonic stem cell differentiation. *Biol Eng.*, 7:7, 2013.

[17] Zhang, X., Liu,Y., Fan,T., Hu ,N., Yang, Z., Chen, X., Wang, Z. & Yang, J. Design and Performance of a Portable and Multichannel SPR Device. *Sensors*, 17:1435, 2017.

[18] Li, J., Han, D., Zeng, J., Deng, J., Hu, N. & Yang, J. Multi-channel surface plasmon resonance biosensor using prism-based wavelength interrogation. *Optics Express*, 14007, 2020.

[19] Kim. N.H., Choi. M, Kim. T. W.; Choi W., Park S.Y.; Byun K. M. Sensitivity and Stability Enhancement of Surface Plasmon Resonance Biosensors Based on a Large-Area Ag/MoS2 Substrate. *Sensors*, 19:1894, 2019.

[20] Tokel, O., Yildiz, U.H., Inci, F., Durmus, N.G., Ekiz, O.O., Turker, B., Cetin, C., Rao, S., Sridhar, K., Natarajan, N. and Shafiee, H. Portable microfluidic integrated plasmonic platform for pathogen detection. *Sci. Rep*., 5:9152, 2015.

[21] Sathiyamoorthy, K., Ramyaa, B., Murukeshan, V.M. & Sun. X. W. Modified two prism SPR sensor configurations to improve the sensitivity of measurement. *Sensors and Actuators A. Physical*, 191:73-77, 2013.

[22] Boruah, R., Mohanta, D., Choudhury, A., Nath, P. & Ahmed, G.A. Surface plasmon resonance-based protein bio-sensing using a Krestschmann configured double prism arrangement. *IEEE Sensors Journal*, 15:6791–6796, 2015.

[23] Puzari, U., & Mukherjee, A. K. Recent developments in diagnostic tools and bioanalytical methods for analysis of snake venom: A critical review. *Analytica Chimica Acta*, 1137: 208-224, 2020.

[24] Warrell, D. A., Gutiérrez, J. M., Calvete, J. J., & Williams, D. New approaches & technologies of venomics to meet the challenge of human envenoming by snakebites in India. *Indian Journal of Medical Research*, 138(1): 38-59, 2013.

[25] Mukherjee, A. K., Kalita, B., Dutta, S., Patra, A., Maiti, C. R., & Punde, D. Snake envenomation: Therapy and challenges in India. *Handbook of venoms and toxins of reptiles; Mackessy S. P., Ed.; CRC Press: Boca Raton, Florida, USA*: 581-592, 2021.

[26] Chippaux, J. P. Snakebite envenomation turns again into a neglected tropical disease!. *Journal of venomous animals and toxins including tropical diseases*, 23: 38, 2017.

[27] Rojnuckarin, P. Clinical Uses of Snake Antivenoms. *Toxinology: Clinical Toxinology in Asia Pacific and Africa; Gopalakrishnakone, P., Faiz, A., Fernando, R., Gnanathasan, C. A., Habib, A.G., Yang, C.C. (Eds); Springer: Netherlands*: 437–452, 2015.

[28] Giri, S., Taye, S. J., Shyam, R., Saikia, B., Jangid, R., Yasmin, R., & Doley, R. Recurrent neurotoxity in Naja kaouthia envenomation: A case report from Assam, India. *Toxicon*, 222: 106990, 2023.

[29] Morarka, A., Agrawal, S., Kale, S., Kale, A., Ogale, S., Paknikar, K., & Bodas, D. Quantum dot based immunosensor using 3D circular microchannels fabricated in PDMS. *Biosensors and Bioelectronics*, 26(6): 3050-3053, 2011.

[30] Kang, K., Oh, S., Yi, H., Han, S., & Hwang, Y. Fabrication of truly 3D microfluidic channel using 3D-printed soluble mold. *Biomicrofluidics*, 12(1), 2018.

[31] Hung, D. Z., Liau, M. Y., & Lin-Shiau, S. Y. The clinical significance of venom detection in patients of cobra snakebite. *Toxicon*, 41(4): 409-415, 2003.

[32] Sanhajariya, S., Duffull, S. B., & Isbister, G. K. Pharmacokinetics of snake venom. *Toxins*, 10(2): 73, 2018.

[33] Yasmin, R., Chanchal, S., Ashraf, M. Z., & Doley, R. Daboxin P, a phospholipase A2 of Indian Daboia russelii venom, modulates thrombin-mediated platelet aggregation. *Journal of Biochemical and Molecular Toxicology*, 37(11): e23476, 2023.

[34] Gahlaut, S. K., Pathak, A., Gupta, B. D., & Singh, J. P. Portable fiber-optic SPR platform for the detection of NS1-antigen for dengue diagnosis. *Biosensors and Bioelectronics*, 196: 113720, 2022.

[35] Shrivastava, A., & Gupta, V. B. Methods for the determination of limit of detection and limit of quantitation of the analytical methods. *Chronicles of Young Scientists*, 2(1): 21-25, 2011.

[36] Mukhtar, W. M., Ahmad, F. H., Samsuri, N. D., & Murat, N. F. Study on plasmon absorption of hybrid Au-GO-GNP films for SPR sensing application. In *AIP Conference Proceedings*, vol. 1972(1), 2018. AIP Publishing.

[37] Weng, G., Li, J., & Zhao, J. Enhanced resonance light scattering of antibody covalently conjugated gold nanoparticles due to antigen-antibody interaction induced aggregation. *Nanoscience and Nanotechnology Letters*, 5(8): 872-878, 2013.

[38] Aslan, K., Luhrs, C. C., & Pérez-Luna, V. H. Controlled and reversible aggregation of biotinylated gold nanoparticles with streptavidin. *The Journal of Physical Chemistry B*, 108(40): 15631-15639, 2004.

[39] Aslan, K., & Pérez-Luna, V. H. Surface modification of colloidal gold by chemisorption of alkanethiols in the presence of a nonionic surfactant. *Langmuir*, 18(16): 6059-6065, 2002.

[40] Schmitt, J., Mächtle, P., Eck, D., Möhwald, H., & Helm, C. A. Preparation and optical properties of colloidal gold monolayers. *Langmuir*, 15(9): 3256-3266, 1999.

[41] Eck, D., Helm, C. A., Wagner, N. J., & Vaynberg, K. A. Plasmon resonance measurements of the adsorption and adsorption kinetics of a biopolymer onto gold nanocolloids. *Langmui*r, 17(4): 957-960, 2001.

[42] Monteiro, J. I., Mukherji, S., & Kundu, T. Development of a low-cost portable Surface Plasmon Resonance Biosensor. In *2013 Annual International Conference on Emerging Research Areas and 2013 International Conference on Microelectronics, Communications and Renewable Energy*, pages 1-5, 2013. IEEE.

[43] Lin, J. H., Sung, W. C., Liao, J. W., & Hung, D. Z. A rapid and international applicable diagnostic device for cobra (genus Naja) snakebites. *Toxins*, 12(9): 572, 2020.

[44] Manson, E. Z., Mutinda, K. C., Gikunju, J. K., Bocian, A., Hus, K. K., Petrílla, V., ... & Kimotho, J. H. Development of an inhibition enzyme-linked immunosorbent assay (ELISA) prototype for detecting cytotoxic three-finger toxins (3ftxs) in African spitting cobra venoms. *Molecules*, 27(3): 888, 2022.

[45] Ramana, L. N., Mathapati, S. S., Salvi, N., Khadilkar, M. V., Malhotra, A., Santra, V., & Sharma, T. K. A paper microfluidic device based colorimetric sensor for the detection and discrimination of elapid versus viper envenomation. *Analyst*, 147(4): 685-694, 2022.